arXiv:1506.07103v3 [cond-mat.mtrl-sci] 24 Feb 2016

First principles many-body calculations of electronic structure and optical properties of SiC nanoribbons

Naresh Alaal[1,2,3]

[1]IITB-Monash Research Academy, CSE Building 2^{nd} Floor, IIT Bombay, Mumbai 400076, India
[2]Department of Physics, Indian Institute of Technology Bombay, Mumbai 400076, India
[3]Department of Materials Engineering, Monash University, Clayton, Victoria 3800, Australia

Vaideesh Loganathan [2]

[2]Department of Physics, Indian Institute of Technology Bombay, Mumbai 400076, India

Nikhil Medhekar [3]

[3]Department of Materials Engineering, Monash University, Clayton, Victoria 3800, Australia

Alok Shukla [2,*]

[2]Department of Physics, Indian Institute of Technology Bombay, Mumbai 400076, India

E-mail: `shukla@phy.iitb.ac.in`

Abstract.

A first principles many-body approach is employed to calculate the band structure and optical response of nanometer sized ribbons of SiC. Many-body effects are incorporated using the GW approximation, and excitonic effects are included using the Bethe-Salpeter equation. Both unpassivated and hydrogen passivated armchair SiC nanoribbons are studied. As a consequence of low dimensionality, large quasiparticle corrections are seen to the Kohn-Sham energy gaps. In both cases quasiparticle band gaps are increased by up to 2 eV, as compared to their Kohn-Sham energy values. Inclusion of electron-hole interactions modifies the absorption spectra significantly, giving rise to strongly bound excitonic peaks in these systems.The results suggest that hydrogen-passivated armchair SiC nanoribbons have the potential to be used in optoelectronic devices operating in the UV-Vis region of the spectrum. We also compute the formation energies of these nanoribbons as a function of their widths, and conclude that hydrogen-saturated ribbons will be much more stable as compared to the bare ones.

PACS numbers: Insert suggested PACS numbers here.

1. Introduction

Successful synthesis of graphene[1], and discovery of its extraordinary electronic properties such as high electron mobility and electrical conductivity[2, 3, 4], has tremendously enhanced research interest in the field of low-dimensional systems, in general, and graphene-like two-dimensional (2D) systems, in particular. One of the drawbacks of graphene is the fact that it is a zero bandgap semiconductor, which limits its applications in electronic devices. Therefore, it is of great interest to discover novel low-dimensional materials which share the attractive properties of graphene, but, in addition, also have a finite band gap. One such candidate, monolayer of hexagonal boron nitride (h-BN) known as 'white graphene', has been successfully synthesized[5] using mechanical exfoliation and chemical vapor deposition techniques, and electrically it is a large bandgap insulator. Nanotubes and nanoribbons of boron nitride have been synthesized and studied[6, 7, 8, 9]. Carbon and silicon are the two most interesting elements in group IV because of their abundance which leads to low costs, and also because of the fact that their allotropes possess attractive electronic properties. Like carbon, silicon also forms a honeycomb structure called silicene which, not only has been studied theoretically[10], but also has been experimentally synthesized in high vacuum conditions [11, 12]. Si, unlike C, prefers the sp^3 hybridization, therefore, silicene, in contrast with graphene, has a buckled bilayer structure. Furthermore, it has not been possible to synthesize silicene in free-standing form, thus, limiting its potential for device applications.

Just like carbon, it is well known that the bulk SiC has several allotropes, although a layered graphitic one has not been experimentally realized so far. However, theoretical calculations have shown that graphitic SiC can be realized by using the technique of "extreme hole injection"[13]. Therefore, it is conceivable that it can also be isolated in a monolayer form, similar to graphene [14, 15]. Because of the fact that basic unit of SiC contains two different atoms, corresponding monolayer will exhibit a finite band gap. Similarly, it may be possible to synthesize SiC-based nanostructures such as nanoribbons, nanotubes, and nanodisks etc [14, 15]. From the applications point of view, SiC nanostructures will have the advantage that their integration into the present Si based technology will be relatively easier. Keeping this in mind, in this work we undertake a systematic electronic structure study of SiC nanoribbons (SiCNRs). Next, we briefly review the existing studies of SiC, and related structures.

Consistent with the intuition, various electronic structure studies have predicted SiC monolayer to be a semiconductor with a band gap of 2.5 eV[16, 17, 18, 19, 20, 21, 22, 23, 24, 25]. Although, SiC monolayer has not been realized in the laboratory as yet, the ultra thin graphitic SiC, which exhibits light emitting properties, has recently been synthesized [26]. SiC micro ribbons [27], crystaline 3C - SiC nanobelts [28], bicrystalline SiC nanobelts [29], and crystalline SiC nanoribbons[30] have been successfully synthesized. Nanowires of SiC have been synthesized by reacting SiO with carbon nanotubes at different temperatures[31]. First principles calculations have shown that hydrogenation of graphitic SiC can lead to formation of stable SiC nanotubes[32].

As far as theory is concerned, SiC nanoribbons (SiCNRs) have been studied extensively using the density-functional theory (DFT) based first-principles methodology [17, 33, 34, 35, 36, 18, 37, 38, 39, 40, 41]. Sun *et al.*[17] studied hydrogen passivated SiCNRs using Perdew-Wang functional (PW91) under the generalized-gradient approximation (GGA) exchange correlation scheme. They found that hydrogen passivated armchair SiCNRs (ASiCNRs) are semiconducting with a direct bandgap, which oscillates and exhibits a gradual overall increase with the width. For the nanoribbons studied, they reported Kohn-sham band gaps in the range 2.3–2.4 eV [17]. Sun *et al.*[17] also found that unlike their graphene counterparts, hydrogen-passivated zigzag SiCNRs (ZSiCNRs) have non degenerate spins, and were near half metallic, with the smaller gap being a few meVs, while the larger one being close to 0.6 eV. The ferri-magnetic state was reported to be most stable, with an anti parellel spin orientation between the two edges [17]. Bekaroglu *et al.*,[18] based upon their first-principles DFT-GGA calculations, reported that bare ASiCNRs have indirect band gaps in the range 1.3–1.7 eV. The same authors[18] as well as Morbec *et al.*[41] studied the influence of vacancies on the electronic structure of SiCNRs using the DFT-GGA approach, and found that single (Si and C) vacancies induce magnetism in non-magnetic ASiCNRs, and double (Si and C) vacancies induce magnetism in ZSiCNRs. Tang *et al.* [40] studied bare-edge and half bare-edge ZSiCNRs using the DFT-GGA approach and reported that the bare-edge ZSiCNRs exhibit magnetic metallic behavior, while half bare edge ZSiCNRs are magnetic semiconductors with small band gap. Oxygen and sulfur terminated ZSiCNRs were studied by Lopez-Benzanilla *et al.*[37] using DFT based local spin-density approximation (LSDA), and observed that ZSiCNRs can be tuned from half metallic to semiconducting. The influence of substitution of edge Si and C atoms with B and N atoms in ZSiCNRs was studied by Zheng *et al*[38] using the DFT-GGA approach, and they found that such substituted ZSiCNRs exhibit semicounducting behavior. The influence of doping on the electronic and magnetic properties of SiCNRs have also been studied by Costa *et al.* [39], who showed that the N doped ZSiCNRs are metallic.

Generally speaking nanoribbons of various materials show interesting properties that are vastly different from those of their bulk counterparts due to quantum confinement. The bandgap in armchair nanoribbons (ANRs) oscillates over three families according to their width, and approaches a value close to that of the parent 2D sheet for large widths [42, 17, 43]. Zigzag nanoribbons(ZNRs) of both graphene and SiC are spin polarized, and the individual spin gaps can be controlled by application of an electric field directed along the width[44, 34, 43]. These unique properties of nanoribbons help to tune the band gap on the basis of their widths, and the edge geometries. Therefore, a good knowledge of their electronic and optical properties is essential for their utilization in opto-electronic devices.

It is a well known fact that the standard DFT based approaches normally underestimate the band gaps of bulk semiconductors because they do not include the quantum many-body effects[45]. However, neglecting many-body effects in low-dimensional systems such as nanoribbons are likely to cause much more severe errors as compared to bulk systems, because electron-correlation effects are enhanced in lower dimensions [46, 47, 48, 49, 50]. All the aforementioned electronic structure studies of SiCNRs have been based upon DFT with various exchange-correlation functionals without accounting for the many-body effects. Furthermore, it will also be of tremendous interest to explore the optical absorption in SiCNRs in order to explore the possibilities of their applications in opto-electronic devices. With these goals in mind, in this work we present a systematic study of ASiCNRs in which we go beyond the mean field DFT approach to compute the influence of many-body effects on their band structure within the GW approximation. We find significant GW corrections of up to 2 eV to the Kohn-Sham band gaps. Furthermore, we also calculate the optical absorption spectra of these systems within a Bethe-Salpeter equation (BSE) based approach, which includes electron-hole interaction, and thus excitonic effects. The absorption spectra of ASiCNRs are found to be dominated by strongly bound exciton peaks with binding energies up to 2eV. We also performed calculations of formation energies of these nanoribbons for various widths, and conclude that with the increasing widths nanoribbons become more stable, and, for a given width, hydrogen-satured ribbons are much more stable as compared to the bare ones.

2. Computational Details

In earlier works from our group we studied the opto-electronic properties of graphene nanoribbons using a semi-empirical Hamiltonian based methodology[51, 52]. In the present calculations, we have adopted a plane-wave based first-principles methodology as implemented in the ABINIT package.[53, 54] First, the calculations were performed for the ground state of the nanoribbon concerned, using DFT-GGA methodology, employing Perdew, Burke, Enzerhof (PBE) pseudopotentials.[55] During the geometry optimization, a kinetic energy cutoff of 26 Hartree (1 Hatree = 27.21 eV) was used, while for Brillouin zone integration, a k-point grid with $1 \times 1 \times 11$ points was employed. For total energy/cell, convergence threshold of 10^{-10} Hartree (Ha) was used, and during the structural relaxations, atomic force cutoff of 5×10^{-5} Ha/Bohr was employed. Once the geometry optimization was complete, charge density profiles, and denisty of states, were computed using the software package VASP,[56] employing the same exchange-correlation potential, and the kinetic energy cutoff as in ABINIT, but a superior k-point mesh of dimensions $1 \times 1 \times 45$. The GGA wave functions are a good starting point for the many body perturbation theoretic computations, aimed at including the electron-correlation effects. The screening effects are included within a plasmon pole approximation, [57] and quasiparticle corrections to the GGA eigenvalues are then evaluated using the G0W0 approximation.[58] For the exchange and correlation parts of self energy calculations, cut off energies of 18 Ha, and 6 Ha, respectively, were used. A $1 \times 1 \times 30$ k-point grid ensured convergence of the GW band gap to within 0.1 eV for the systems considered here. A total of 250 bands was employed for the GW calculations, out of which the number of virtual (unoccupied) bands was > 150. Thus, the choice of computational parameters employed in the GW calculations suggests that these calculations are well converged. Lastly, the BSE is solved to obtain the optical response with the inclusion of the electron-hole interaction, retaining only the resonant part of the Bethe-Salpeter Hamiltonian, because the inclusion of the coupling had a negligible effect. In the GW and the BSE calculations, a Coulomb truncation scheme was also used to avoid the consideration of long range interactions between the periodic images. Nanoribbons were taken to be periodic along the z direction, and to represent an isolated system, vacuum separations of more than 11 Å were taken between the adjacent unit cells along both x and y directions.

To denote the widths of the nanoribbons, the usual index notation is used. ASiCNRs are prefixed by the number of dimer (bond) lines, N_a, along the width of the ribbon (N_a-H-ASiCNR is used for H-passivated, and N_a-ASiCNR used for bare armchair nanoribbons). In this work, we have studied ribbons with $4 \leq N_a \leq 12$, which for H-ASiCNRs corresponds to widths between 0.7 nm and 2.3 nm, and for bare ASiCNRs to widths between 0.46 nm and 1.7 nm.

.

3. Results and Discussion

In this section we present the results of our calculations on the quasiparticle band structure and the optical absorption spectra of ASiCNRs. Before that, however, we use the same methodology to compute the band structure of 2D SiC sheet at the GW level, in order to validate our approach.

3.1. SiC Monolayer

Because the calculations presented here are the first reported GW calculations on ASiCNRs, it is important to benchmark the underlying approach. Therefore, we first use the same methodology to compute the quasi-particle band structure of monolayer SiC for which GW calculations had been reported earlier by Louie and coworkers [21]. The honeycomb structure adopted for the infinite SiC sheet is shown in Fig. 1(a), while its calculated GW band structure is presented in Fig. 1(b). We obtain a direct band gap of 3.4 eV located at the K point of Brillouin zone, at the GW level, which is 0.9 eV greater than our DFT-GGA band gap of 2.5 eV. Our GW result is found to be in very good quantitative agreement with the GW value of 3.6 eV, also located at the K point, reported by Louie group [21]. Furthermore, we also calculated excitonic binding energy of 2D SiC sheet using the GW+BSE approach. Fig 1 (c) shows the optical absorption spectra of sheet, with (red curve), and without (blue curve), electron-hole interactions. The difference between the first prominent peaks of these two curves gives the binding

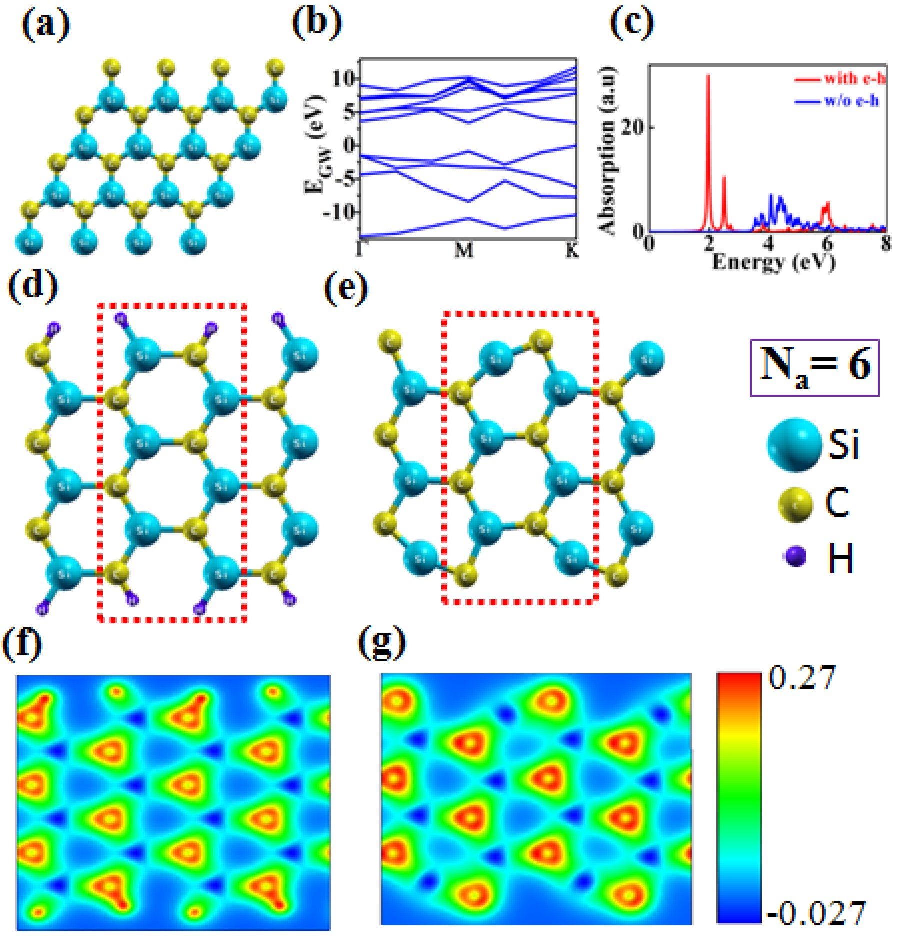

Figure 1. (Color online) Geometric structures of (a) 2D SiC sheet (d) Hydrogen passivated, (e) bare armchair SiC nanoribbons, . Both types of SiCNRs correspond to $N_a = 6$, and unit cells employed for the calculations are shown in the dashed boxes. Panels (b) and (c) show the calculated GW band structure and optical absorption spectra of SiC sheet. Panels (f) and (g) display 2D charge density (in the units of e/Bohr^3) plots of 6-H-ASiCNR, and 6-ASiCNR, respectively.

energy of 1.5 eV, which is 0.3 eV more than the value 1.2 eV reported by Louie and coworkers[21]. This agreement between the GW and BSE calculations performed using two different packages, assures us of the quality of our calculations.

3.2. Quasiparticle energies of hydrogenated armchair SiC nanoribbons

First we present and discuss the results of hydrogen-passivated ASiCNRs (H-ASiCNRs), for which three different families of width, that is, $N_a = 3p$, $N_a = 3p{+}1$, and $N_a = 3p{+}2$ (p an integer), have been studied, with N_a ranging from 4 to 12. The geometrical structure of H-ASiCNR for $N_a = 6$ is shown in Fig. 1(d), for which our optimized average Si-C bond length is 1.78 Å, while Si-H and C-H bond lengths are 1.49 Å and 1.09 Å, respectively. Table 1 presents the band gaps at the GGA and GW levels,

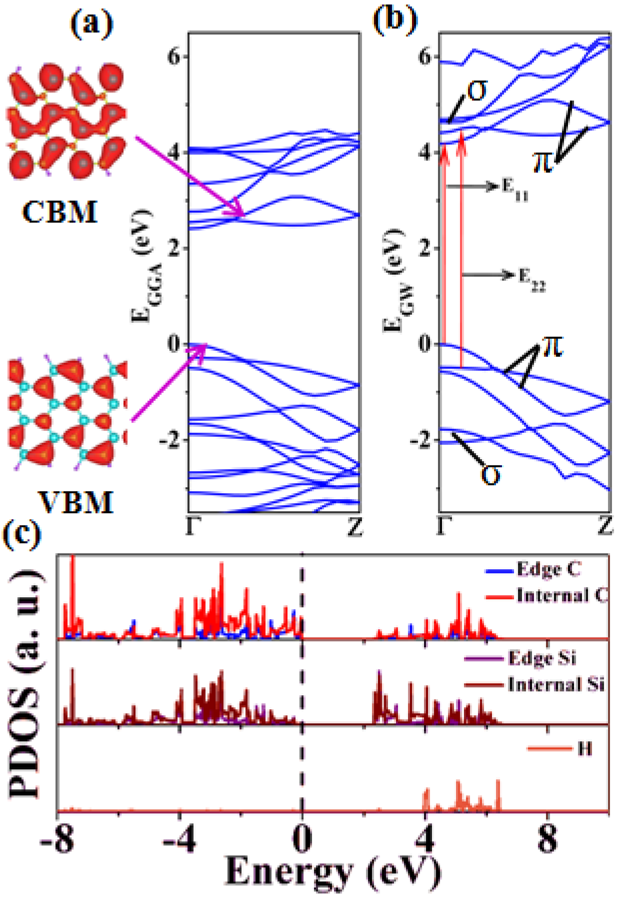

Figure 2. (Color online) For 6-H-ASiCNR: (a) DFT-GGA band structure (pink arrows show the charge densities corresponding to VBM and CBM) (b) GW band structures (red arrows denote interband transitions). σ/π character of bands is also pointed out. (c) Atom projected density of states (black dashed line denotes the Fermi level)

and the exciton binding energies for N_a= 6, 7, 8. The GW self-energy corrections increase their band gaps by 1.6-1.8 eV, when compared to their GGA values. Thus, the magnitude of the increase in band gaps for H-ASiCNRs due to electron correlation effects is significantly greater than the 1 eV increase observed in the monolayer discussed in the previous section, and for the increase reported for the bulk SiC [21]. The larger correction observed for nanoribbons is a consequence of enhanced Coulomb interaction effects, and reduced screening, in lower dimensions.

Next, we specifically discuss the case of 6-H-ASiCNR (notation N_a-H-ASiCNR), because the other two studied H-ASiCNRs exhibit similar behavior. In Figs. 2 (a) and 2 (b), we present our calculated GGA and GW quasiparticle band structures of 6-H-ASiCNR, from where it is clear that the hydrogen passivated ASiCNRs are direct band gap semiconductors as their valence band maximum (VBM) and conduction band minimum (CBM) occur at the high symmetrical point Γ in brillioun zone. Partial charge

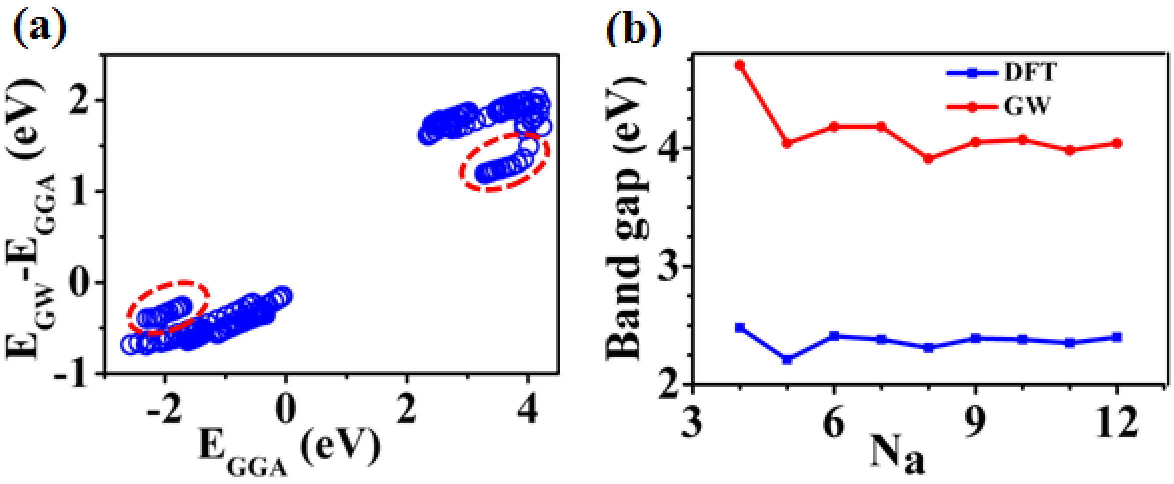

Figure 3. (Color online) (a) Quasiparticle self-energy corrections to the GGA Kohn-Sham energies. Corrections to the nearly free electron states are enclosed by ellipses (red-dashed), and (b) variation of the GGA band gap and quasiparticle gaps with ribbon width for H-ASiCNRs.

denisty plots for VBM and CBM of 6-H-ASiCNRs are shown in left side panel of Fig 2 (a). These plots reveal that main contribution to the VBM charge density is from electrons distributed around the carbon atoms, while electrons from from both Si and C atoms contribute to the CBM charge density. Fig. 2 (c) shows the atom projected density of states (PDOS) of 6-H-ASiCNR. PDOS has been plotted both for internal atoms, as well as the ones located on the edges. It clearly show that edge and internal C atoms contribute mainly to the states states near to the VBM, while internal Si atoms contribute dominantly to form the states close to the CBM. The contribution of hydrogen atoms appears in the conduction band states far away from the CBM. The self energy corrections to various bands are plotted in Fig. 3 (a), and are dependent on their nature. The π band states associated with the p_z orbitals are perpendicular to the ribbon plane, extending into the vacuum region. As a result, the many body interactions for the π states are less screened, and lead to large quasiparticle corrections. On the other hand, the σ band states lie in the plane of the ribbon, and experience greater screening. Thus, the quasiparticle corrections for the σ states are smaller than the π states. In H-ASiCNRs, the bands around the Fermi energy comprise only of the π states, which exhibit corrections which are mostly linear as a function of the energy. A few points (encircled, *cf.* Fig. 3a) which deviate from the main linear region correspond to the nearly free electron states which are loosely bound to the ribbon, and have weak many-body interactions resulting in smaller quasiparticle corrections [47]. Compared to their GGA shapes, the bands not only shift, but also stretch by an average 30%–40%, and even cross due to the non-uniform quasiparticle corrections resulting from the GW calculations. The family behavior of the band gaps is preserved at the GW level, as the correction is roughly proportional to the GGA band gap. Fig. 3(b) shows the band gap as a function of the ribbon width in GGA and GW approximation for H-ASiCNRs.

From Table 1 it is obvious that the family behaviour of DFT and GW band gaps follow the heirachy $3p > 3p+1 > 3p+2$, in good agreement with earlier studies of DFT band gaps of H-ASiCNRs,[17] and quite unlike H terminated graphene [46] and boron-nitride [49] nanoribbons which follow the hierarchy $3p+1 > 3p > 3p+2$

N_a	E_{GGA}	E_{GW}	ΔE	E_b
6 ($3p$)	2.41	4.18	1.77	1.07
7 ($3p+1$)	2.38	4.17	1.79	1.76
8 ($3p+2$)	2.31	3.91	1.60	1.93

Table 1. The values of GGA and quasiparticle band gaps and their difference for H-ASiCNRs are tabulated. The last column gives the highest exciton binding energy. All energy values are in eV.

3.3. Optical absorption spectra of H-ASiCNRs

Based on GW quasiparticle band structures, we calculated optical absorption spectra of H-ASiCNRs, with (GW-BSE), and without (GW-RPA) electron-hole interaction, and results are presented in Fig. 4. BSE calculations were performed by including five valence and five conduction bands. The polarization direction of the radiation is assumed to be along the length of the ribbons, as significant quenching occurs in 1D systems for perpendicular directions. The blue colored curves denote the absorption due to inter-band transitions at the GW-RPA level. The red colored curve denotes the absorption obtained by solving the Bethe Salpeter equation, including both the electron-electron, and electron-hole interactions.

As compared to the independent particle absorption spectra, BSE based spectra exhibit changes both in the positions of the peaks, as well as the line shapes, with excitonic states having binding energies in the range 1.07–1.93 eV. We adopt the following notation to label interband transitions: E_{nm} denotes the interband transitions from the nth valence band to the mth conduction band, with the band indices counted from the Fermi level. The underlying band-to-band transitions are also marked with arrows in the band structure plot in Fig. 2 (b). The first peak (E_{11}) of ribbon arises due transitions between the highest valence band, and the lowest conduction band at the zone center, while other prominent peak arises due to transitions between the second valence and conduction bands. Weak peaks in between include contributions from cross transitions between these bands. For the case of $N_a = 6, 7$, E_{22} peak is the most intense one, while for $N_a = 8$ case, E_{11} peak acquires significant oscillator strength, and becomes the most intense peak. The binding energies of the excitons corresponding to the E_{11} peak are 1.07 eV, 1.76 eV, and 1.93 eV, and for $N_a = 6,\ 7,$ and 8, respectively. In

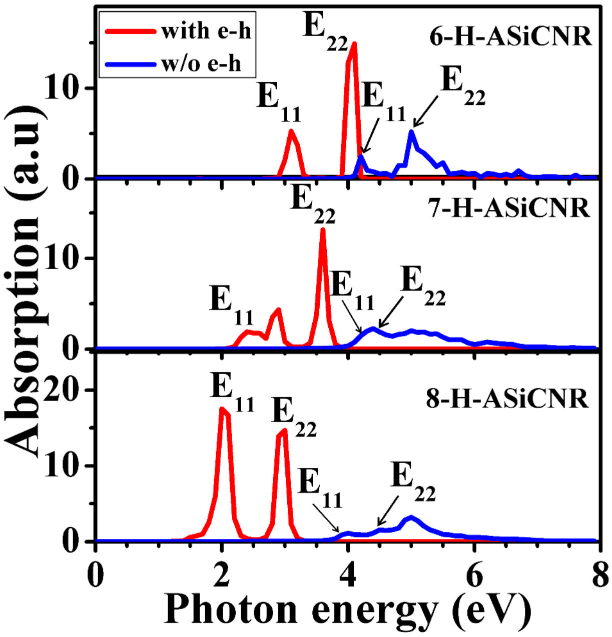

Figure 4. (Color online) Optical absorption spectra of the H-ASiCNRs, with (red) and without (blue) electron-hole interaction. Lorentzian broadening of 0.03 eV has been used.

comparison, our computed value of exciton binding energy of SiC sheet is 1.5 eV, while that of bulk 2H-SiC is reported to be 0.1 eV[21]. Thus, exciton binding energy for ASiCNRs is comparable to that of the monolayer, but significantly larger than that of the 3D bulk SiC. This large difference between the exciton binding energies of ASiCNRs and bulk SiC can be attributed to their reduced dimensionality, because in reduced dimensions, electron-hole interactions get stronger as quantum confinement increases the overlap between electron and hole wave functions, leading to the formation of small radius excitons[49]. When we compare the exciton binding energies of nanoribbons of different widths, we find a strong width dependence, implying that the strength of electron-hole interactions is also strongly width dependent. This suggests that one can tune the opto-electronic properties of H-ASiCNRs, which are direct band gap materials, by manipulating their width, a property highly useful from the point of view of device applications.

3.4. Quasiparticle energies of bare armchair SiC nanoribbons

In this section, we present and discuss the quasi-particle band structure of bare ASiCNRs. Fig 1 (e) displays the relaxed geometric structure of bare 6-ASiCNR, from which it is obvious that it undergoes significant edge reconstruction because of the dangling bonds, and the Si-C bond length at the edge is reduced from 1.78 Å to 1.69 Å. The effect of edge reconstruction is also obvious in total charge density plot of the ground states of bare 6-ASiCNRs (Fig. 1 (g)), when compared with that of 6-H-ASiCNR (Fig. 1 (f)). Furthermore, we find that, at all levels of theory, for the same width, the band gaps of bare ASiCNRs are smaller as compared to those of H-ASiCNRs.

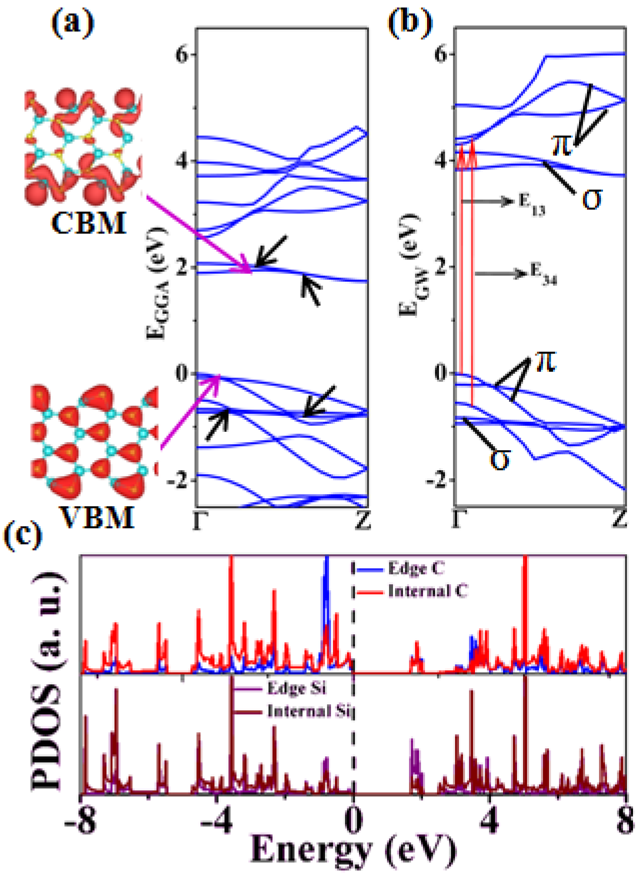

Figure 5. (Color online) (a) DFT-GGA, and (b) GW band structures of bare 6-ASiCNR. Red color arrows denote the interband transitions, pink color arrows show the VBM and CBM, black color arrows denote the additional valence and conduction bands. σ/π character of bands is also pointed out. (c) Partial density of states for 6-ASiCNR, Fermi level shown with black dashed lines.

At the DFT-GGA level, they are smaller by $\approx$0.7 eV , a result in agreement with the results of previous theoretical studies,[18] while at the GW level, the difference reduces to $\approx 0.3-0.4$ eV. For bare ASiCNRs also we studied the family behavior by considering widths of N_a= 6 (3p), 7 (3p+1), 8 (3p+2);, the results of our calculations are presented in the Table 2. Figure 5 displays the calculated GGA and GW band structures for $N_a = 6$. From the figure and the table it is obvious that, as in the case of hydrogen-passivated ribbons, quasiparticle corrections due to the GW approach broaden the band gaps of bare ASiCNRs also by about 2 eV. However, unlike the hydrogen-passivated ribbons, the bare ASiCNRs exhibit an indirect band gap because the top of the valence band, and the bottom of the conduction band, are located at points Γ and Z of the Brillouin zone, respectively, whereas in H-ASiCNRs both were located at the Γ point. As shown in Fig. 5, as compared to H-ASiCNRs, for the case of bare ASiCNRs we can observe that two new, relatively flatter bands, appear near both the CBM and the VBM. As far as the CBM region is concerned, it is now entirely composed of these two new bands, while for the valence band case, the new bands are slightly away from the VBM. This restructuring of the band structure caused by hydrogen removal leads not only to a reduced band gap, but also transforms bare ASiCNRs into indirect band gap materials, as compared to H-ASiCNRs. Charge density analysis reveals that these additional valence and conduction bands are due to the dangling edge bonds, and, because, the electrons involved do not participate in the bond formation, they have relatively less interaction with each other, leading to flatter bands. Partial charge desity plots for VBM and CBM of bare ASiCNRs are presented in Fig 5 (a). A comparison with the corresponding plots of H-ASiCNRs reveals that: (a) VBMs of bare ribbons are similar to the case of hydrogen saturated ones in that they derive their charge density contributions from the same set of carbon atoms, and (b) CBMs of bare ribbons are entirely different from those of the saturated ones in that their charged density is almost entirely due to the edge silicon atoms. From the PDOS plots of bare ASiCNRs presented in Fig 5 (c), one can deduce that the main contribution to the states near VBM is from interior C atoms, while the contribution to the states near CBM is mainly due to the edge Si atoms.

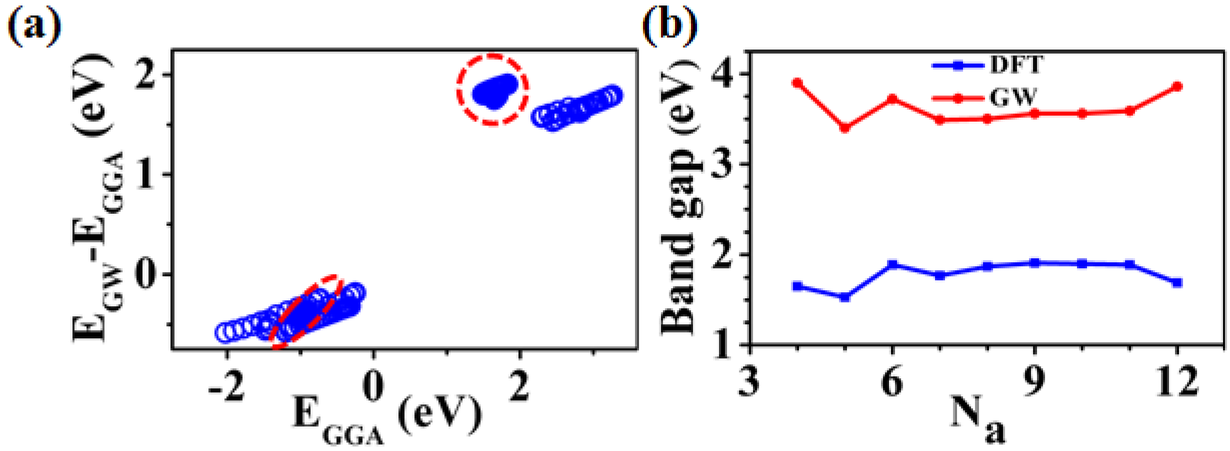

Figure 6. For bare ASiCNRs: (a) quasi-particle self-energy corrections to the GGA Kohn-Sham energies. Corrections to the states corresponding to flat bands in conduction (valence) band regions are enclosed inside red-dashed circle (ellipse). (b) Variation of the GGA and quasi-particle band gaps as a function of the ribbon width.

In Fig. 6(a), we show the self energy corrections for ASiCNRs, as a function of energies. The corrections to the GGA eigenvalues of bare ribbons are qualitatively similar to those for H-ASiCNRs, with the corrections to the π states being larger, as compared to those for the σ states, and exhibit a linear variation with respect to the energy. The states enclosed in red circle, which deviate from the main region, represent corrections to the conduction band states localized on the edge atoms. In Fig. 6(b) we present the variation of the band gap as a function of the ribbon width, and it is clear that bare ASiCNRs follow the same trends as H-ASiCNRs in that the band gap exhibits oscillatory behavior. For the largest width considered ($N_a = 12$), GW band gap of H-ASiCNR is 0.64 eV larger than that of the SiC sheet, while for bare ribbon the same difference is 0.46 eV. With the increasing width, band gaps of hydrogen passivated nanoribbons are expected to approach the band gap of the SiC monolayer, while in case of bare ones it is unlikely, because of the presence of flat bands (Fig.5(a)).

N	E_{GGA}	E_{GW}	ΔE	E_b
6 ($3p$)	1.74	3.72	1.98	0.62
7 ($3p+1$)	1.51	3.48	1.97	1.26
8 ($3p+2$)	1.62	3.56	1.94	2.48

Table 2. Values of GGA and GW band gaps, and their difference for bare ASiCNRs are tabulated. The last column gives the highest exciton binding energy for the given width. All energies are in eV units.

3.5. Optical absorption spectra of bare ASiCNRs

In Fig. 7 we present the optical absorption spectrum of bare ASiCNRs, for $N_a = 6$–8. For the calculations of the BSE spectra, five valence and five conduction bands were included. As for the case of H-ASiCNRs, once the electron-hole interaction effects are incorporated, the resulting BSE spectrum of bare ribbons looks completely different as compared to the band-to-band absorption spectrum computed at the GW-RPA level. Similar to the case of H-ASiCNRs, the excitons in bare ribbons are also strongly bound, with the binding energies in bare ribbons, for the same ribbon widths, being larger than in the hydrogen passivated ones (*cf.* Tables 1 and 2). We can also find strongly bound excitons in bare ASiCNRs with binding energies of in the range 0.62–2.45 eV. The reasons behind these large binding energies are the same as in case of H-ASiCNRs, i.e., stronger electron-hole interactions due to quantum confinement, and reduced screening in lower dimensions.

One qualitative difference in the optical properties of bare ribbons as compared to the hydrogen-passivated ones is that bare ribbons do not absorb at the band gap because they exhibit an indirect band gap, as discussed in the previous section. Therefore, the prominent peaks displayed in Fig. 7 do not have an E_{11} contribution. In all the ribbons considered, the first peak corresponds to an E_{13} transition, while the strongest peak is due to E_{34} transition. Because of the indirect nature of excitons, bare ASiCNRs cannot be used in devices such as LEDs, however, they may be useful in transport oriented applications. As far as the location of first absorption peak is concerned, both hydrogen-passivated and bare nanoribbons follow the pattern $E(3p+2) > E(3p+1) > E(3p)$. Because of the presence of an indirect band gap in bare ASiCNRs, these materials will have poor photoluminscence efficiency, and thus will not be useful in light-generation applications.

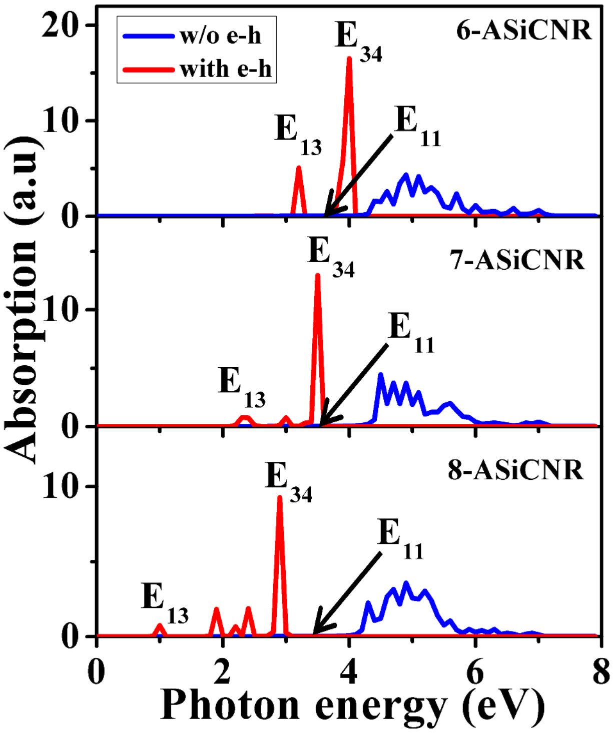

Figure 7. Optical absorption spectrum of bare 6-ASiCNRs, with (GW-BSE), and without (GW-RPA), electron-hole interactions. Lorentzian broadening of 0.03 eV has been used.

3.6. Energetic Stability

Energetic stability of hydrogen terminated ASiCNRs is well known from previous theoretical studies.[17] In order to check the stability of bare ASiCNRs, we performed calculations of their formation energies, and compared them with those of H-ASiCNRs . Following formula was employed for computing the edge formation energy per unit length of edge of a given nanoribbon,

$$E_f = \left(E_c - N_d E_{2D} - 0.5 N_H E_{H_2}\right)/2L,$$

where E_c is the total energy/cell of the nanoribbon under consideration, E_{2D} is the total energy/cell of infinite 2D SiC sheet, E_{H_2} is the total energy of a hydrogen molecule, N_d is the total number of SiC units in the unit cell, N_H is the total number of H atoms in the unit cell ($N_H = 0$, for bare nanoribbons), while L is the length of the edge (in Å unit). It is easy to see that a lower value of E_f will imply a higher stability of the considered nanoribbon.

Formation energy as a function of nanoribbon width for both bare and H-saturated nanoribbons studied here is presented in Fig 8. The fact that both types of nanoribbons exhibit little change in the value of edge formation energy with the increasing width, implies a weak width dependence. H-ASiCNRs studied here have a much lower average formation energy of 0.07 eV/Å as compared to 0.76 eV/Å of the bare ones, clearly

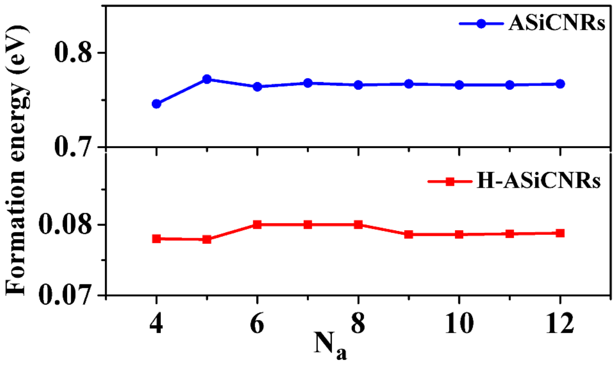

Figure 8. Formation energies of bare ASiCNRs and H-ASiCNRs as a function of width

demonstrating that H-ASiCNRs will be much more stable when compared to the bare ones. Therefore, based upon the formation energy data, we conclude that the synthesis of H-ASiCNRs in laboratory will be much more favourable as compared to the bare ones.

4. Conclusions

To summarize, we performed large-scale first-principles calculations on armchair-type SiC nanoribbons of widths in the range $4 \leq N_a \leq 12$, in order to study their electronic structure and optical properties. Both hydrogen passivated and bare edge configurations were considered, sophisticated many-body methods such as the GW approximation for the band structure, and BSE for the optical absorption, were adopted, and the convergence of the calculations was carefully checked. Therefore, the results presented here are fairly accurate, and constitute, to the best of our knowledge, the first set of GW and BSE calculations for SiCNRs. From our calculations we conclude that hydrogen-passivated ribbons are direct band gap semiconductors, and bare edge-ribbons undergo significant edge reconstruction, and become indirect band gap semiconductors. As expected, self-energy corrections widened the band gaps, and excitonic effects modified optical absorption spectra dramatically for both the H-saturated and the bare ribbons. Our results predict that quasiparticle band gaps of hydrogen passivated and bare ASiCNRs are ≈ 2 eV larger than their DFT-GGA band gaps, due to the inclusion of many-body effects within the GW approximation. These large quasiparticle corrections to the band gaps suggest enhanced Coulomb correlation effects in reduced dimensions. Our BSE based calculations of the excitonic effects predict large excitonic binding energies in the range of 0.62–2.45 eV in optical absorption spectra of both types of ASiCNRs, which is yet another consequence of reduced dimensions. Key results of our calculations can be tested in future experiments once these nanoribbons are synthesized in laboratories. Theoretically speaking, it will also be of interest to explore other ribbon geometries of SiC, and also ribbons with unequal proportions of Si and C.

Acknowledgements

All authors gratefully acknowledge computaional support from Monash Sun Grid cluster and the National Computing Infrastucture, Australia. N.A. gratefully thanks P. Chan and S. Ayyub for helping in allocating the required CPUs to carry out the calculations.

[1] Novoselov K S, Geim A K, Morozov S V, Jiang D, Zhang Y, Dubonos S V, Grigorieva I V and Firsov A A 2004 *Science* **306** 666–669 (*Preprint* `http://www.sciencemag.org/content/306/5696/666.full.pdf`) URL `http://www.sciencemag.org/content/306/5696/666.abstract`

[2] Geim A K and Novoselov K S 2007 *Nature materials* **6** 183–191

[3] Katsnelson M I 2007 *Materials today* **10** 20–27

[4] Castro Neto A H, Guinea F, Peres N M R, Novoselov K S and Geim A K 2009 *Rev. Mod. Phys.* **81**(1) 109–162 URL `http://link.aps.org/doi/10.1103/RevModPhys.81.109`

[5] Coleman J N, Lotya M, ÓNeill A, Bergin S D, King P J, Khan U, Young K, Gaucher A, De S, Smith R J *et al.* 2011 *Science* **331** 568–571

[6] Chopra N G, Luyken R J, Cherrey K, Crespi V H, Cohen M L, Louie S G and Zettl A 1995 *Science* **269** 966–967 (*Preprint* `http://www.sciencemag.org/content/269/5226/966.full.pdf`) URL `http://www.sciencemag.org/content/269/5226/966.abstract`

[7] Lee R S, Gavillet J, Chapelle M L d l, Loiseau A, Cochon J L, Pigache D, Thibault J and Willaime F 2001 *Phys. Rev. B* **64**(12) 121405 URL `http://link.aps.org/doi/10.1103/PhysRevB.64.121405`

[8] Park C H and Louie S G 2008 *Nano Letters* **8** 2200–2203 (*Preprint* `http://pubs.acs.org/doi/pdf/10.1021/nl080695i`) URL `http://pubs.acs.org/doi/abs/10.1021/nl080695i`

[9] Guo G Y and Lin J C 2005 *Phys. Rev. B* **72**(7) 075416 URL `http://link.aps.org/doi/10.1103/PhysRevB.72.075416`

[10] Ni Z, Liu Q, Tang K, Zheng J, Zhou J, Qin R, Gao Z, Yu D and Lu J 2011 *Nano letters* **12** 113–118

[11] Fleurence A, Friedlein R, Ozaki T, Kawai H, Wang Y and Yamada-Takamura Y 2012 *Phys. Rev. Lett.* **108**(24) 245501 URL `http://link.aps.org/doi/10.1103/PhysRevLett.108.245501`

[12] Feng B, Ding Z, Meng S, Yao Y, He X, Cheng P, Chen L and Wu K 2012 *Nano Letters* **12** 3507–3511 pMID: 22658061 (*Preprint* `http://dx.doi.org/10.1021/nl301047g`) URL `http://dx.doi.org/10.1021/nl301047g`

[13] Miyamoto Y and Yu B D 2002 *Applied physics letters* **80** 586–588

[14] Menon M, Richter E, Mavrandonakis A, Froudakis G and Andriotis A N 2004 *Phys. Rev. B* **69**(11) 115322 URL `http://link.aps.org/doi/10.1103/PhysRevB.69.115322`

[15] Mavrandonakis A, Froudakis G E, Schnell M and Mühlhäuser M 2003 *Nano Letters* **3** 1481–1484 (*Preprint* `http://pubs.acs.org/doi/pdf/10.1021/nl0343250`) URL `http://pubs.acs.org/doi/abs/10.1021/nl0343250`

[16] Lin X, Lin S, Xu Y, Hakro A A, Hasan T, Zhang B, Yu B, Luo J, Li E and Chen H 2013 *Journal of Materials Chemistry C* **1** 2131–2135

[17] Sun L, Li Y, Li Z, Li Q, Zhou Z, Chen Z, Yang J and Hou J 2008 *The Journal of chemical physics* **129** 174114

[18] Bekaroglu E, Topsakal M, Cahangirov S and Ciraci S 2010 *Phys. Rev. B* **81**(7) 075433 URL `http://link.aps.org/doi/10.1103/PhysRevB.81.075433`

[19] Lu T Y, Liao X X, Wang H Q and Zheng J C 2012 *J. Mater. Chem.* **22**(19) 10062–10068 URL `http://dx.doi.org/10.1039/C2JM30915G`

[20] Ding Y and Wang Y 2013 *The Journal of Physical Chemistry C* **117** 18266–18278

[21] Hsueh H C, Guo G Y and Louie S G 2011 *Phys. Rev. B* **84**(8) 085404 URL `http://link.aps.org/doi/10.1103/PhysRevB.84.085404`

[22] Baumeier B, Krüger P and Pollmann J 2007 *Phys. Rev. B* **76**(8) 085407 URL `http://link.aps.org/doi/10.1103/PhysRevB.76.085407`

[23] Şahin H, Cahangirov S, Topsakal M, Bekaroglu E, Akturk E, Senger R T and Ciraci S 2009 *Phys.*

Rev. B **80**(15) 155453 URL http://link.aps.org/doi/10.1103/PhysRevB.80.155453

[24] Wu I J and Guo G Y 2007 *Phys. Rev. B* **76**(3) 035343 URL http://link.aps.org/doi/10.1103/PhysRevB.76.035343

[25] Zhao K, Zhao M, Wang Z and Fan Y 2010 *Physica E: Low-dimensional Systems and Nanostructures* **43** 440 – 445 ISSN 1386-9477 URL http://www.sciencedirect.com/science/article/pii/S1386947710004972

[26] Lin S S 2012 *The Journal of Physical Chemistry C* **116** 3951–3955 (*Preprint* http://pubs.acs.org/doi/pdf/10.1021/jp210536m) URL http://pubs.acs.org/doi/abs/10.1021/jp210536m

[27] Yushin G N, Cambaz Z G, Gogotsi Y, Vyshnyakova K L and Pereselentseva L N 2008 *Journal of the American Ceramic Society* **91** 83–87 ISSN 1551-2916 URL http://dx.doi.org/10.1111/j.1551-2916.2007.02093.x

[28] Xi G, Peng Y, Wan S, Li T, Yu W and Qian Y 2004 *The Journal of Physical Chemistry B* **108** 20102–20104

[29] Wu R, Wu L, Yang G, Pan Y, Chen J, Zhai R and Lin J 2007 *Journal of Physics D: Applied Physics* **40** 3697 URL http://stacks.iop.org/0022-3727/40/i=12/a=023

[30] Zhang H, Ding W, He K and Li M 2010 *Nanoscale research letters* **5** 1264–1271

[31] Sun X H, Li C P, Wong W K, Wong N B, Lee C S, Lee S T and Teo B K 2002 *Journal of the American Chemical Society* **124** 14464–14471

[32] Alfieri G and Kimoto T 2014 *Applied Physics Letters* **104** 033107

[33] Lou P and Lee J Y 2009 *The Journal of Physical Chemistry C* **113** 12637–12640 (*Preprint* http://pubs.acs.org/doi/pdf/10.1021/jp903155r) URL http://pubs.acs.org/doi/abs/10.1021/jp903155r

[34] Lou P and Lee J Y 2009 *The Journal of Physical Chemistry C* **113** 21213–21217 (*Preprint* http://pubs.acs.org/doi/pdf/10.1021/jp906558y) URL http://pubs.acs.org/doi/abs/10.1021/jp906558y

[35] Ding Y and Wang Y 2012 *Applied Physics Letters* **101** 013102 URL http://scitation.aip.org/content/aip/journal/apl/101/1/10.1063/1.4732786

[36] Lou P 2013 *J. Mater. Chem. C* **1**(17) 2996–3003 URL http://dx.doi.org/10.1039/C3TC30173G

[37] Lopez-Bezanilla A, Huang J, Kent P R C and Sumpter B G 2013 *The Journal of Physical Chemistry C* **117** 15447–15455 (*Preprint* http://dx.doi.org/10.1021/jp406547a) URL http://dx.doi.org/10.1021/jp406547a

[38] Zheng F L, Zhang Y, Zhang J M and Xu K W 2011 *physica status solidi (b)* **248** 1676–1681 ISSN 1521-3951 URL http://dx.doi.org/10.1002/pssb.201147001

[39] Costa C and Morbec J 2011 *Journal of Physics: Condensed Matter* **23** 205504

[40] Tang Z K, Wang L L, Tang L M, Huang W Q, Zhang D Y, Xu L and Li X F 2013 *Solid State Communications* **158** 25 – 28 ISSN 0038-1098 URL http://www.sciencedirect.com/science/article/pii/S0038109813000203

[41] Morbec J M and Rahman G 2013 *Phys. Rev. B* **87**(11) 115428 URL http://link.aps.org/doi/10.1103/PhysRevB.87.115428

[42] Son Y W, Cohen M L and Louie S G 2006 *Phys. Rev. Lett.* **97**(21) 216803 URL http://link.aps.org/doi/10.1103/PhysRevLett.97.216803

[43] Zhang Z and Guo W 2008 *Phys. Rev. B* **77**(7) 075403 URL http://link.aps.org/doi/10.1103/PhysRevB.77.075403

[44] Son Y W, Cohen M L and Louie S G 2006 *Nature* **444** 347–349

[45] Godby R W, Schlüter M and Sham L J 1986 *Phys. Rev. Lett.* **56**(22) 2415–2418 URL http://link.aps.org/doi/10.1103/PhysRevLett.56.2415

[46] Prezzi D, Varsano D, Ruini A, Marini A and Molinari E 2008 *Phys. Rev. B* **77**(4) 041404 URL http://link.aps.org/doi/10.1103/PhysRevB.77.041404

[47] Yang L, Cohen M L and Louie S G 2007 *Nano Letters* **7** 3112–3115 (*Preprint* http://pubs.acs.org/doi/pdf/10.1021/nl0716404) URL http://pubs.acs.org/doi/abs/10.

1021/nl0716404

[48] Yang L, Cohen M L and Louie S G 2008 *Phys. Rev. Lett.* **101**(18) 186401 URL `http://link.aps.org/doi/10.1103/PhysRevLett.101.186401`

[49] Wang S, Chen Q and Wang J 2011 *Applied Physics Letters* **99** 063114

[50] Hu C, Ogura R, Onoda N, Konabe S and Watanabe K 2012 *Phys. Rev. B* **85**(24) 245420 URL `http://link.aps.org/doi/10.1103/PhysRevB.85.245420`

[51] Gundra K and Shukla A 2011 *Physical Review B* **83** 075413

[52] Gundra K and Shukla A 2011 *Physical Review B* **84** 075442

[53] Gonze X, Amadon B, Anglade P M, Beuken J M, Bottin F, Boulanger P, Bruneval F, Caliste D, Caracas R, Ct M, Deutsch T, Genovese L, Ghosez P, Giantomassi M, Goedecker S, Hamann D, Hermet P, Jollet F, Jomard G, Leroux S, Mancini M, Mazevet S, Oliveira M, Onida G, Pouillon Y, Rangel T, Rignanese G M, Sangalli D, Shaltaf R, Torrent M, Verstraete M, Zerah G and Zwanziger J 2009 *Computer Physics Communications* **180** 2582 – 2615 ISSN 0010-4655 URL `http://www.sciencedirect.com/science/article/pii/S0010465509002276`

[54] Gonze X 2005 *Zeitschrift für Kristallographie* **220** 558–562

[55] Fuchs M and Scheffler M 1999 *Computer Physics Communications* **119** 67–98

[56] Kresse G and Furthmller J 1996 *Computational Materials Science* **6** 15 – 50 ISSN 0927-0256 URL `http://www.sciencedirect.com/science/article/pii/0927025696000080`

[57] Godby R W and Needs R J 1989 *Phys. Rev. Lett.* **62**(10) 1169–1172 URL `http://link.aps.org/doi/10.1103/PhysRevLett.62.1169`

[58] Onida G, Reining L and Rubio A 2002 *Rev. Mod. Phys.* **74**(2) 601–659 URL `http://link.aps.org/doi/10.1103/RevModPhys.74.601`